A Model-Based Algorithm for Designing Suboptimal Morphological Filters for Restoring Subtractive-Noise-Corrupted Images

by

Ian R. Joughin,
Robert M. Haralick
Electrical Engineering Department
University of Washington

Edward R. Dougherty
Center for Imaging Science
Rochester Institute of Technology

Keywords: mathematical morphology, optimal filters, restoration, nonlinear image processing.

Abstract Simple optimization procedures are used to obtain optimal filters based on the Matheron expansion for binary images corrupted by subtractive noise. The Matheron expansion allows us to represent all morphological filters as either a union of erosions or an intersection of dilations. We perform a search over a subset of the filters represented by the union-of-erosions version of the Matheron expansion. We present results for a set of simple binary images with regular borders and a more complex set with very irregular borders. Results are compared against results for binary closings.

1 Introduction

Noise manages to corrupt most images in one way or another. As a result, a common problem in image processing is filtering a noisy image to recover the original. Linear filters are well understood. In addition, they are easy to design and analyze. Classical Wiener filtering provides a mathematically simple and computationally efficient optimization process. Unfortunately, linear filters often blur edges and introduce other types of distortion. Nonlinear methods, while more intractable than linear methods, tend to have many desirable properties, such as the ability to preserve edges. There are no simple optimal-filtering methods for nonlinear filters, such as Wiener filtering. Optimal nonlinear filters are often found by computationally intensive search procedures.

A number of papers have been written on the subject of optimal nonlinear filtering. For instance, Coyle *et al.* present theoretical and experimental results for optimal stack filtering of gray-scale images [1][2], and Schonfeld and Goutsias derive optimal morphological sequences of openings and closings for binary images based on the pattern spectrum [3]. Our interest focuses on the approach of Dougherty [4] [5], who derives several results for optimal binary and gray-scale morphological filters based on the Matheron expansion. This representation originally was introduced by Matheron [6]. Maragos [7] and Giardina and Dougherty [8] give several variations on the theorem for both binary and gray-scale images defined on both continuous and digital domains. With these representations, filters are expressed as either a union/max of erosions or as an intersection/min of dilations for binary/grayscale images.

As presented, the methodology of [4] presents an intractable search for optimal structuring elements if one wishes to consider even moderately large structuring elements. To mitigate the search problem, Loce and Dougherty [9] [10] have employed various optimization constraints, search strategies, and error representations. Most relevant to the current approach is library optimality [9], where only structuring elements contained in some a priori library are examined for filter goodness.

Most relevant to the optimization routine developed herein is the model-based approach of Dougherty and Haralick [11], who model classes of images in terms of the holes within them and model noisy images in terms of the new holes created by hole-creating noise processes. The intent of [11] is to develop a "spectral-like" approach akin to frequency-based Wiener-type filtering. As the Wiener

filter weights the spectrum of the noisy image to a produce mean-square-error-optimal estimate of the uncorrupted signal, the method of [11] examines the therein-defined "hole-spectrum" to derive an optimal morphological filter (based on the Matheron expansion). Although there is an algorithmic paradigm discussed in theoretical terms [11], it is tied to the hole spectrum and is not actually implemented. For completeness, we mention that Haralick *et al.* [12] have presented a model-based Wiener-type approach to opening filters based on the opening spectrum. This approach, however, is not immediately relevant herein because it does not utilize the Matheron expansion.

As in [11], we focus on holes created by a subtractive noise process. We relax the model requirements, however, by postulating only a noise-process model and not an uncorrupted-image model. The cost is a lack of mathematical elegance and a spectral formulation of the filter; the gain is a simple and practical nonlinear-optimization procedure for restoration of images corrupted by subtractive noise.

In Section 2 we briefly discuss the basic morphological operations of erosion and dilation and introduce the Matheron expansion theorem and discuss its various properties. In Section 3 we discuss our optimization procedure for binary images corrupted by subtractive noise. Optimal filters are derived for two sets of images and experimental results are presented in Section 4. In the final sections we discuss the performance of our algorithm and some of the extensions required for other noise models.

2 Morphological Preliminaries

If E is the set of numbers used for the row column coordinates of a binary image, then a binary image F is a subset of $E \times E$. Dilation is defined as

$$\begin{aligned} F \oplus K &= \{x \mid \text{ for some } f \in F \text{ and } k \in K, x = f + k\} \\ &= \bigcup_{k \in K} F_k, \end{aligned}$$

where $F \subseteq E \times E$, $K \subseteq E \times E$. The set K is referred to as the structuring element. The notation F_k denotes the set obtained by adding k to each point of F. The set F_k is the translation of the set F by the point k. Erosion of a binary image F by a structuring element K is defined as

$$\begin{aligned} F \ominus K &= \{x \mid \text{ for every } k \in K, x + k \in F\} \\ &= \bigcap_{k \in K} F_{-k}. \end{aligned}$$

A morphological opening is defined as an erosion followed by dilation,

$$F \circ K = (F \ominus K) \oplus K,$$

and a morphological closing is defined as a dilation followed by an erosion,

$$F \bullet K = (F \oplus K) \ominus K.$$

For further reference see Giardina and Dougherty [8].

A binary-image-to-binary-image mapping is denoted by $\Psi : E \times E \rightarrow E \times E$. A mapping Ψ is said to be a τ-mapping if it is translation invariant. That is, if $\Psi(F_x) = \Psi(F)_x$. A mapping is said to be increasing if $F \subset G$ implies $\Psi(F) \subset \Psi(G)$. Increasing τ-mappings are an important class of filters. Erosion, dilation, opening, and closing are increasing τ-mappings. Increasing τ-mappings are also called "morphological filters" [8].

The kernel of an increasing τ-mapping Ψ [6][7][8] consists of all the sets F where the origin is contained in $\Psi(F)$,

$$Ker(\Psi) = \{F : \{0\} \in \Psi(F)\}. \tag{1}$$

The following representation theorem [7][8] is originally attributed to Matheron [6]. If $\Psi : E \times E \rightarrow E \times E$ is an increasing τ-mapping, it possesses a representation

$$\Psi(F) = \bigcup_{K \in Ker(\Psi)} F \ominus K. \tag{2}$$

The kernel of Ψ is far too large to make this realization of Ψ computationally practical. The function Ψ can be realized as an expansion over a basis set Bas[Ψ] rather than the kernel. The basis for the kernel [8] is a subset of the kernel. The members of a basis set must satisfy two conditions [8]. These conditions are

1. If $F, G \in$ Bas[Ψ], then $F \not\subseteq G$ and $G \not\subseteq F$;
2. For any $F \in$Ker[Ψ] there exists $G \in$Bas[Ψ] such that $G \subseteq F$.

Dougherty and Giardina show that if a basis exists, it is unique [13]. They also provide a bound on the number of elements in the basis. This bound is dependent upon the size of the domain of the image being filtered. The number of elements in the basis is usually a manageable size. If not, the basis can often be truncated with reasonable approximate results. Dougherty [4] [5] presents an approach where optimization is performed by searching over sets of bases.

A function Ψ that satisfies the above conditions can also be represented by an intersection of dilations (Matheron [6]). If $\Psi : E \times E \rightarrow E \times E$ is an increasing τ-mapping, it possesses a representation

$$\Psi(F) = \bigcap_{K \in Ker(\Psi^*)} F \oplus K. \tag{3}$$

The dual of Ψ denoted as Ψ^* and is given as [8]

$$\Psi^*(F) = (\Psi(F^c))^c. \tag{4}$$

3 Optimal Morphological Filtering For Subtractive Noise

We wish to design a filter to restore a class of images with similar structural features that are corrupted by noise with known statistics. The noise process is one that creates holes in the images. Our algorithm incorporates knowledge of the structure of the images through a representative set of ideal training images $\{F_1, F_2, \ldots F_M\}$.

The noise is modeled as a set of possible hole shapes $\{N_1, N_2, \ldots N_I\}$ with an associated probability distribution. The set of possible hole shapes that may occur is assumed to be finite and their probability distribution known. It is also assumed that holes with respect to a given structuring element K, do not interfere with each other. Noninterference with respect to a structuring element K means that any hole dilated by K has an empty intersection with every other hole. This is the set of noise modeling assumptions used in our optimization algorithm. These assumptions compose the full set of our model assumptions (compare to [11]). While they often will not be completely satisfied, filters derived under the model perform well so long as the noninterfering hypothesis is only moderately violated. This robustness relative to moderate interference is consistent with respect to grain overlapping reported in other morphological studies ([3][12][14][15]). The performance of filters optimized under these assumptions will not be greatly affected by an increased variety of hole shapes and interference among holes present in real images.

With this model the noisy $\tilde{F}$ image can be represented by

$$\tilde{F} = F - N = F \cap N^c, \tag{5}$$

where F is an ideal image. The noise N can be represented as

$$N = \bigcup_{i=1,2\ldots}^{I} N_i \oplus \{x_{i_1}, x_{i_2}, \ldots\}, \tag{6}$$

where the N_i belong to the set of hole shapes $\{N_1, N_2, \ldots N_I\}$, and $\{x_{i_1}, x_{i_2}, \ldots\}$ are sets of randomly distributed points determined by the hole distribution and underlying point process.

In some cases, hole interference effects will be too great to ignore. One way around this problem is to augment the set of noise shapes $\{N_1, N_2, \ldots N_I\}$ to include some of the interference. If single-point noise is considered, the set of noise shapes consists of just a single-point hole. By considering the probabilities that these holes fall together to create larger holes, the noise model can be adjusted to account for holes with two points, three points etc.

With subtractive noise, all the points of the noisy image belong to the ideal image. We wish to restore the missing points. To do this, we use the union-of-erosions form of the Matheron expansion. With this form, the single-point structuring element consisting of the origin is always used as one

element in the expansion. This erosion is just an identity operation, and it ensures that all points of the noisy image are included in the output. Then, other erosions in the union are used to restore the missing points.

An example of how a single erosion fills a hole is shown in Figure 1. Since the origin has been included as a structuring element, the rest of the structuring elements do not include the origin due to basis requirement (1): that each basis structuring element cannot be contained in any other basis structuring element. A point x belonging to a hole at z ($x \in N_z$) is filled when all the points of the translated structuring element K_x fit into the noisy image ($K_x \subset \tilde{F}$).

Instead of optimizing by searching over sets of bases [4][5][9][10], we build a basis with a simple best-first search. At each step in the search, we choose the structuring element with the minimum cost. In order to obtain a basis, structuring elements are chosen so that they meet the conditions 1 and 2 for members of a basis. It is not computationally possible to search over all possible structuring elements. For example, the number of structuring elements that are contained within a 5×5 grid is 25×2^{25}. As with the library approach [9][10], we limit our search to structuring elements that intuitively seem to be good at fixing holes. With this method, we hand pick a set of N (several hundred) structuring elements $\{K_1, K_2, \ldots K_N\}$ over which we execute the search.

In choosing structuring elements, we must consider their connectedness or disconnectedness. Structuring elements that are good at filling holes are often, but not always, disconnected sets. This is because, in addition to how well a structuring element fills holes, we must consider how much a structuring element degrades the noise free image (see [9] [11]). Figure 2 shows how two-point disconnected (K_1) and connected (K_2) structuring elements both fix a hole equally well but K_2 overfills along the right edge. This is because the erosion of an image by a connected structuring element not containing the origin translates the image so that part of it falls outside the border of the original image. Disconnected structuring elements can be chosen to translate the image in opposing directions and then intersect. As a result, most of the erosion falls within the boundary of the original image. Another consideration is the amount of overfilling a structuring element does. Structuring elements that fix holes well but tend to overfill can often be modified by the addition of a few points so that they still do a good job of fixing but overfill far fewer points.

In our algorithm we want to be able to determine for a noisy image $\tilde{F}$ with a hole N_f, whether f belongs to $\tilde{F} \ominus K$. One way to determine this is to actually erode $\tilde{F}$ by K. This method is inefficient, however, since we wish to consider a large number of such cases, and performing an erosion for each case is far too computationally expensive. A more efficient method is to use the result of the following proposition that specifies under what conditions a given pixel $f \notin \tilde{F}$ will be included in $\tilde{F} \ominus K$.

Proposition: Suppose $\tilde{F} = F \cap N_f^c$. Then ($f \in F \ominus K$ and $f \in N_f{}^c \ominus K$) iff $f \in \tilde{F} \ominus K$.

Proof:

$$f \in N_f^c \ominus K \text{ and } f \in F \ominus K \text{ iff}$$

$$f \in (F \ominus K) \cap (N_f^c \ominus K) \text{ iff}$$

$$f \in (F \cap N_f^c) \ominus K = \tilde{F} \ominus K.$$

By checking whether the noise satisfies $f \in N_f{}^c \ominus K$, and whether the noise-free image satisfies $f \in F \ominus K$, it is possible to determine whether a given point is in $\tilde{F} \ominus K$ without actually eroding the noisy image. The set $F \ominus K$ is an upper bound on the set of points that can be added to the expansion with the use of the structuring element K in the expansion. The set of points that will actually be added are a subset of this set since erosion is an increasing operation and $\tilde{F} \subseteq F$. The second condition states that the origin of the noise shape must be fixable in the infinite plane (i.e. $f \in N_f{}^c \ominus K$). This is the simplest case for a given noise shape since there are no border effects.

Our problem is to determine an optimal filter, given a set of structuring elements $\{K_1, K_2, \ldots K_N\}$, a set of noise shapes $\{N_1, N_2, \ldots N_I\}$ with their associated probabilities of occurrence, and an ideal image F. The image F is assumed to be contained in some given region S, $F \subseteq S$.

In equation (6), the noise process is given as a set of noise shapes, translated to a set of random points $x \in S$. In our algorithm, we evaluate the improvement in restoration gained by the use of each structuring element K in the expansion for every point in each noise shape at every possible translation. These computations are made easier if we augment our set of shapes $\{N_1, N_2, \ldots N_I\}$ so that for each shape N, we consider the shape with the origin at each point in N. For example, a two-point noise shape is now considered twice; once with the origin at each point. This augmented set is denoted by $\mathcal{N} = \{N_1, N_2, \ldots N_J\}$. We can then consider the event N_s (N translated to s) for each $N \in \mathcal{N}$ and each $s \in S$.

The probability of occurrence of a noise shape with its origin translated to a point s belonging to set of noise shapes in the noisy image (6) is denoted $P(N, s)$. We assume that the noise process is stationary so we can define $P(N) = P(N, s)$. Note that these events are mutually exclusive, so summing all the probabilities over the noise shapes yields the probability that a pixel will be lost in the noisy image.

At each step in the search, we evaluate the expected number of additional fixes each potential structuring element K could add to the restoration. A *fix* is defined as the restoration of a point f that is not in the noisy image but is in the original image. After the first step in the search, we count only those fixes that previously chosen structuring elements are not capable of doing. That is, we compute only the net improvement to the restoration gained by the addition of each potential structuring element.

Given that $i-1$ structuring elements, $K_1, K_2, \ldots K_{i-1}$, have been selected, for each unselected structuring element K we would like to know the expected number of net fixes, which we denote by $E[netfixes \mid K, i]$. For each pixel $s \in F$, define the random variable

$$Q(K, i, s) = \begin{cases} 1, & \text{if } s \text{ is fixed by } K \text{ but not by } K_1, K_2, \ldots, K_{i-1} \\ 0, & \text{otherwise} \end{cases}$$

$$= \begin{cases} 1, & \text{if } s \in F - \tilde{F},\ s \in (\tilde{F} \ominus K), \text{ and } s \notin \tilde{F} \ominus K_k \text{ for } k \leq i-1 \\ 0, & \text{otherwise.} \end{cases} \quad (7)$$

Then

$$E[Q(K,i,s)] = P[s \in (F - \tilde{F}) \cap (\tilde{F} \ominus K) \cap \bigcap_{k=1}^{i-1} (\tilde{F} \ominus K_k)^c]. \tag{8}$$

Because we have assumed that each noise shape occurs with the origin at every pixel within it, the event $s \in F - \tilde{F}$ can be partitioned into J mutually exclusive events, $s \in F - N_s$, $N \in \mathcal{N}$. Letting

$$Q'(s,N,K,i) = \begin{cases} 1, & \text{if } Q(K,i,s) = 1 \text{ and } s \in F - N_s \\ 0, & \text{otherwise,} \end{cases} \tag{9}$$

we have

$$\begin{aligned} E[Q(K,i,s)] &= \sum_{N \in \mathcal{N}} E[Q'(s,N,K,i)] \\ &= \sum_{N \in \mathcal{N}} E[Q(K,i,s) \mid s \in N_s] P(N,s) \\ &= \sum_{N \in \mathcal{N}} E[Fix(s,N,K,i)] P(N), \end{aligned} \tag{10}$$

where

$$Fix(s,N,K,i) \equiv \begin{cases} 1, & s \in F \ominus K, s \in N_s{}^c \ominus K, \text{ and } s \notin \bigcup_{k=1}^{i-1} \tilde{F} \ominus K_k, \\ 0, & \text{otherwise} \end{cases} \tag{11}$$

$$s \in F, \text{ and } N \in \mathcal{N}.$$

Summing $E[Q(K,i,s)]$ over $s \in F$ gives the expected number of net fixes, so that

$$E[netfixes \mid K,i] = \sum_{s \in F} \sum_{N \in \mathcal{N}} Fix(s,N,K,i) P(N). \tag{12}$$

In addition to the fixes, we must also evaluate the expected number of fills. A *fill* is defined as the addition of a point f to the restored image that did not belong to the original image. As with fixes, at each step in the search we count only those fills that would not have been filled by any of the structuring elements chosen at previous steps. With fills we must also consider the event when no noise occurs at a point. This is because the erosions can introduce fills into the noise-free image. We did not worry about this with fixes because no noise meant that the point was not missing and, therefore, did not need to be fixed due to the inclusion of the origin as structuring element. To account for fills, we define the following function whose domain consists of those points of S not belonging to F

$$Fill(s,N,K,i) \equiv \begin{cases} 1, & s \in F \ominus K, s \in N_s{}^C \ominus K, \text{ and } s \notin \bigcup_{k=1}^{i-1} \tilde{F} \ominus K_k, \\ 0, & \text{otherwise} \end{cases} \tag{13}$$

$$s \in S - F, \text{ and } N \in \mathcal{N} \cup \{\emptyset\}.$$

An analysis similar to that for equation (12) shows the expected number of net fills at each step in the search is

$$E[netfills \mid K, i] = \sum_{s \in S-F} \sum_{N \in \mathcal{N} \cup \{\emptyset\}} Fill(s, N, K, i) P(N). \tag{14}$$

Then we can define a cost function for each K at each step in i the search as

$$J(K, i) = E[netfills \mid K, i] - E[netfixes \mid K, i], \tag{15}$$

where the sign of the cost function has been chosen so that we minimize cost. Using this cost function, the M best $K \in \{K_1, K_2, \ldots K_N\}$ are chosen by using a simple best-first search.

4 Experimental Results

4.1 Images

Two classes of ideal binary images are used to verify our algorithm. The first class consists of images with smooth regular borders and large interior areas. By interior area we mean those pixels not touching border pixels. These images generally consist of only a few connected components. To represent this class, a set of binary machine-part images is used. These images are shown in Figure 3.

The second class of images are those images with irregular borders and relatively little interior area. Such images typically have many irregularly shaped connected components. In these experiments, we use a set of thresholded aerial images of Washington. D.C., which are typical of images in this class. These images are given in Figure 4.

4.2 Structuring Elements

For this set of experiments, we limit the size of the structuring elements to those which are contained within a 5×5 neighborhood. This set consists of 25×2^{25} possible structuring elements, which is still far to large a set to search over. The set is reduced by choosing only structuring elements that seem to be good at fixing holes. Using intuitive selection methods, a set of 582 structuring elements have been chosen. Such an approach is fully analogous to library constraint [9]. The manner of selection used here to form bases from the library, however, is very different from the approach of [9], which is formulated to facilitate the original search strategy of [4]. Also as in [9], to limit the run time of the design algorithm, we limit the basis size by stopping when the gain (according to equation (15)) becomes insignificant. Filter suboptimality results from both the library and size constraints.

4.3 Noise Model

All experiments are based on single-point whitening noise. The ideal images are corrupted by noise with densities of 0.05, 0.1, 0.15, and 0.2. This means if the density is 0.1, a binary-1 pixel has a 1 in 10 chance of being independently changed to a zero. Since the noise is subtractive, binary-0 pixels are unaffected by the noise process.

For training purposes, the noise is assumed to consist of several types of non-overlapping holes. The assumption that the holes do not overlap is an idealization introduced for the optimization process.

In this set of experiments, the noise neighborhoods are modeled as the set of eight-connected holes with three points or less. The probability of a single-point hole p_1 is the probability that a noise point falls with no eight-connected neighbors. If p is the noise density, then $p_1 = p(1-p)^8$. Similarly, each probability of occurrence for the four possible two-point holes is the probability that two independent noise points fall together with no other nearest neighbors. Connected holes with three or more points are considered to be equivalent. The probability of a three-point hole is the probability that a hole occurred that was not a one-or two-point hole.

4.4 Error Criterion Function

The performance of each filter can be evaluated by comparing the average Hamming distance between each filtered noisy image and its associated ideal image. This error is defined as

$$e(F, \tilde{F}) = \#((F \cap \tilde{F}^c) \cup (\tilde{F} \cap F^c)), \tag{16}$$

where F is the ideal image and $\tilde{F}$ is the noisy or filtered image. The $\#$ operator counts the number of points in a set.

4.5 The Experiments

Filters for each image and noise type are generated for a total of eight (2 images $\times$ 4 noise types) filters. One representative image from each set is used for training. The program is run until additional structuring elements yield less than five net fixes (expected number of fixes - expected number of fills). The program also outputs the cost (15) associated with each structuring element. The performance of these filters on the image sets is measured using the error criterion function given above. Noisy images are generated by corrupting the ideal images with noise of the four densities given above.

We used one machine-part and one D.C. image for training. In the machine-part example, performance is evaluated for noisy versions of the training image and three additional images. For

the D.C. example, one image in addition to the training image is used. For each image and noise density, ten noisy images are generated. The error criterion is averaged over the ten results for each image/noise-density pair.

For purposes of comparison, the noisy images are closed with 10 structuring elements: a disk of radius 2, squares with widths from 2-4, and horizontal and vertical lines with lengths 2-4. The results of the best closing for each image are compared against the union-of-erosions output. Like a union of erosions, one of which is the identity, closing by K is an antiextensive filter ($\tilde{F} \bullet K \supset \tilde{F}$) that fills holes. Moreover, as an increasing filter, closing possesses a Matheron representation over its basis. Were we able to fully optimize relative to the Matheron expansion as called for in [4] and were the closing by K optimal, then the optimal Matheron expansion would be the expansion for the closing by K. The algorithm proposed here has several features that lead to suboptimality, so that, even if the closing is optimal, we should not expect to find its Matheron expansion. Our purpose for considering the closing is only for comparison with a well-known filter that is often used to fill holes.

4.6 Results

We used the images in Figures 3a and 4a as our training images. The resulting filters for the machine part images are shown in Figure 5 and the filters for the D.C. images are shown in Figure 6. The performance of these filters was evaluated as described above and the results are given in Table 1.

The results for most of the D.C. images were significantly better for the union-of-erosions filter over the best closing. The improvement is much greater for the lower noise densities. For the highest noise density performance was roughly equivalent with slightly better performance for the union-of-erosions on the training image and slightly better for the closing on the test image. An example of a closed and union-of-erosions filtered image is given in Figure 7.

The data from the D.C. images indicates that closings are better at hole filling at the expense of overfilling, while the union-of-erosions filter does not fill noise holes quite as well but is good at avoiding overfilling. With noise density $N_D = 0.05$, the D.C. images do not have many holes to fill, and the closing actually overfills more than it fixes. The union-of-erosions filter, on the other hand, is able to better discriminate between noise and non-noise holes, resulting in much better performance. The amount of overfilling doesn't change much with increasing noise density, but the number of noise holes does. As the noise density increases, the closing is able to compensate for its overfilling by fixing more holes than the union-of-erosions filter until performance is equivalent at $N_D = 0.20$.

In all cases, the closing results were better for the machine-part images. The results were good for both filters, but in many cases the closing fixed twice as many points as the union-of-erosions filter. A noisy machine part image after closing and union-of-erosions filtering can be seen in Figure 8. The machine part images have much simpler structure than the D.C. images, and there is far less potential for overfilling. In these cases, the superior hole filling ability of the closing is responsible

for the better performance.

Equation (15) gives the cost function for our algorithm, which is the the expected number of fills minus the expected number fixes. This is just the negated net restoration improvement for each step in the search. If we sum the negated values of the cost function for the optimal K for each of the M steps in the search, we obtain the overall net restoration improvement as

$$E[e(F,\tilde{F}) - e(F,F_F)] = \sum_{i=1}^{M} J(K_{i_{opt}}, i),$$

where F_F is the union-of-erosions filtered image. Table 2 gives this expected improvement, as computed by our algorithm, and the values from our experimental results. The expected values were computed under the assumption of noninterfering noise holes, while the measured values are due to a real noise process in which interference could occur. The results in Table 2 show good agreement, with the average difference in the two columns being less than 10 %. This indicates that our assumption of noninterference did not have a great effect on our optimization results, and that we chose an appropriate set of noise shapes with which to model the noise.

Running on a Sun SPARC 1+, the algorithm took approximately 8 to 48 hours to determine each filter. This time represents design time for the filter, not implementation time, which can be under a second for the filters of both Figures 5 and 6 when implemented on appropriate inexpensive hardware, even if, as is usually the case, the erosion unions are implemented serially. The design algorithm is assumed to be off-line.

5 A Comment on Mixed Noise

Owing to the dual Matheron representation in terms of an intersection of dilations, the additive noise problem is similar to the subtractive noise problem. When both additive and subtractive noise are present, however, the problem becomes much more difficult. In this case, it is not possible to consider the noise and image separately to determine if a point will be fixed. To design a union-of-erosions filter, an erosion must be done for each noise shape and image point to determine if the point will be fixed. Without modification to this approach, the added complexity of combined additive and subtractive noise will probably yield an algorithm with unacceptable run times.

6 Conclusion

An algorithm for union-of-erosion filter design has been given to restore images degraded by subtractive noise. The salient point is that it provides a way of constructing (sub)optimal morphological filters via the Matheron expansion by using the image process and the statistics of the noise. It does so by using a relatively simple cost function in conjunction with a prechosen library of structuring

elements from which to choose. Experiments indicate that filter design is fairly robust with respect to the noninterference assumption of the noise model. They also indicate that the suboptimal filters work better than closings when the original image possesses small holes and crevices that are easily overfilled, whereas images that are not easily overfilled might better be restored with closings rather than using the suboptimal procedure.

References

[1] E.J. Coyle, J.-H Lin, M Gabbouj, "Optimal stack filtering and the estimation and structural approaches to image processing," *IEEE Trans. Accous., Speech, Signal Processing,* vol. ASSP-37, pp. 2037-2066, December 1989.

[2] J.-H Lin, E.J. Coyle, "Minimum mean absolute error estimation over the class of generalized stack filters," *IEEE Trans. Accous., Speech, Signal Processing,* vol. ASSP-38, pp. 663-678, April 1990.

[3] D. Schonfeld, J. Goutsias, "Optimal morphological pattern restoration from noisy binary images," *IEEE Trans. Pattern. Anal. Machine Intell.,* vol. 13, pp. 14-29, January 1991.

[4] E.R. Dougherty, "Optimal mean-square n-observation digital morphological filters Part I: Optimal filters," *CVGIP: Image Understanding*, vol. 55, no. 1, pp. 36-54, January 1992.

[5] E.R. Dougherty, "Optimal mean-square n-observation digital morphological filters Part II: Optimal gray-scale filters," *CVGIP: Image Understanding*, vol. 55, no. 1, pp. 55-72, January 1992.

[6] G. Matheron, *Random Sets and Integral Geometry*, New York: Wiley, 1975.

[7] P. Maragos,R. Shafer "Morphological filters – part I: their set-theoretic analysis and relations to linear shift invariant filters," *IEEE Trans. Accous., Speech, Signal Processing,* vol. ASSP-35, pp. 1153-1169, August 1987.

[8] C.R. Giardina, E.R.Dougherty, *Morphological Methods in Image and Signal Processing,* Englewood Cliffs, NJ: Prentice Hall 1988.

[9] R.P. Loce and E.R. Dougherty, "Facilitation of optimal binary morphological filter design via structuring-element libraries and observation constraints," *Journal of Optical Engineering*, vol. 31, no. 5, pp. 1008-1025, May 1992.

[10] R.P. Loce and E.R. Dougherty, "Optimal morphological restoration: the morphological filter mean-absolute-error theorem," *Journal of Visual Communication and Image Representation,* vol. 3, no. 4, pp. 412-432, December 1992.

[11] E.R. Dougherty and R.M. Haralick, "Hole-spectrum representation and model-based optimal morphological restoration for binary images degraded by subtractive noise," *Mathematical Imaging and Vision*, vol. 1, no. 3, pp. 257-278, September 1992.

[12] R.M Haralick, E.R. Dougherty, and P.L. Katz, "Model-based morphology: The opening spectrum," Advances in Image Analysis, Y. Madavieh and R.C. Gonzales, Eds., SPIE Press vol. PM08, Chapter 12, pp. 355-373, 1992.

[13] E. R. Dougherty and C. R. Giardina, "A digital version of the Matheron representation theorem for increasing τ-mappings in terms of a basis for the kernel," *Proc. IEEE Conf. Computer, Vision, Pattern Recogn.*, Miami FL, pp. 534-536, June 1986.

[14] E.R. Dougherty, R.M. Haralick, Y. Chen, C. Agerskov, U. Jacobi, and P.H. Sloth, "Estimation of optimal tau-opening parameters based on independent observation of signal and noise pattern spectra," *Journal of Signal Processing* vol. 29, no. 3, pp. 265-281, December 1992.

[15] F. Sand, and E.R. Dougherty, "Statistics of the morphological pattern-spectrum moments for a random grain model," *Journal of Mathematical Imaging and Vision,* vol. 1, no. 2, pp. 121-135, July 1992.

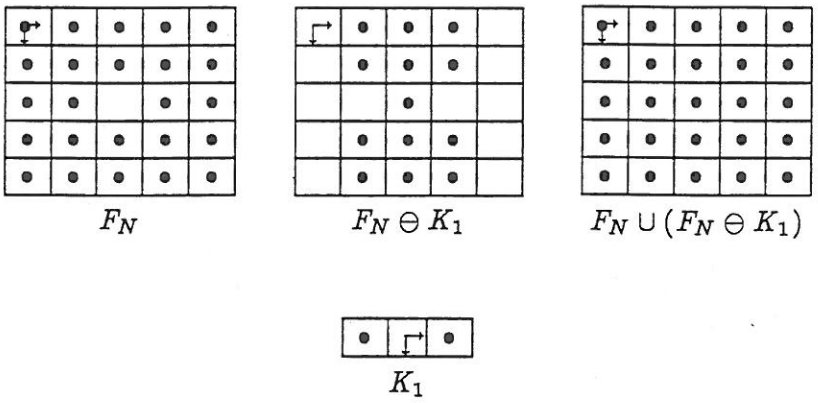

Figure 1: An example of hole filling by union of erosions.

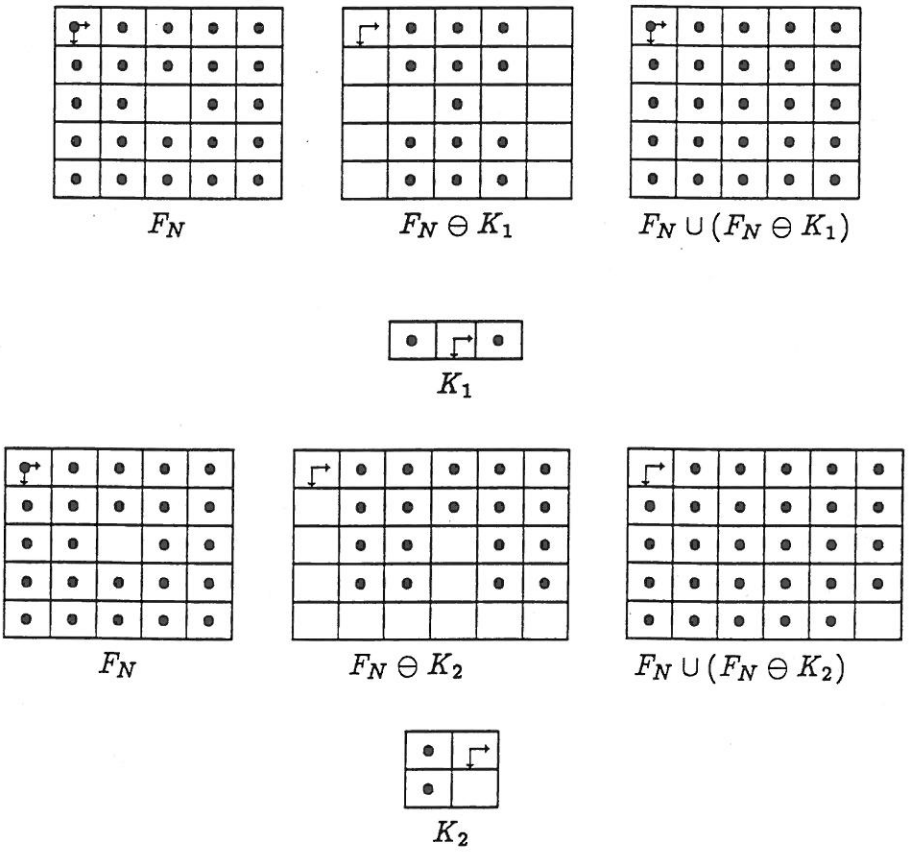

Figure 2: An example of hole filling by a connected and a disconnected structuring element.

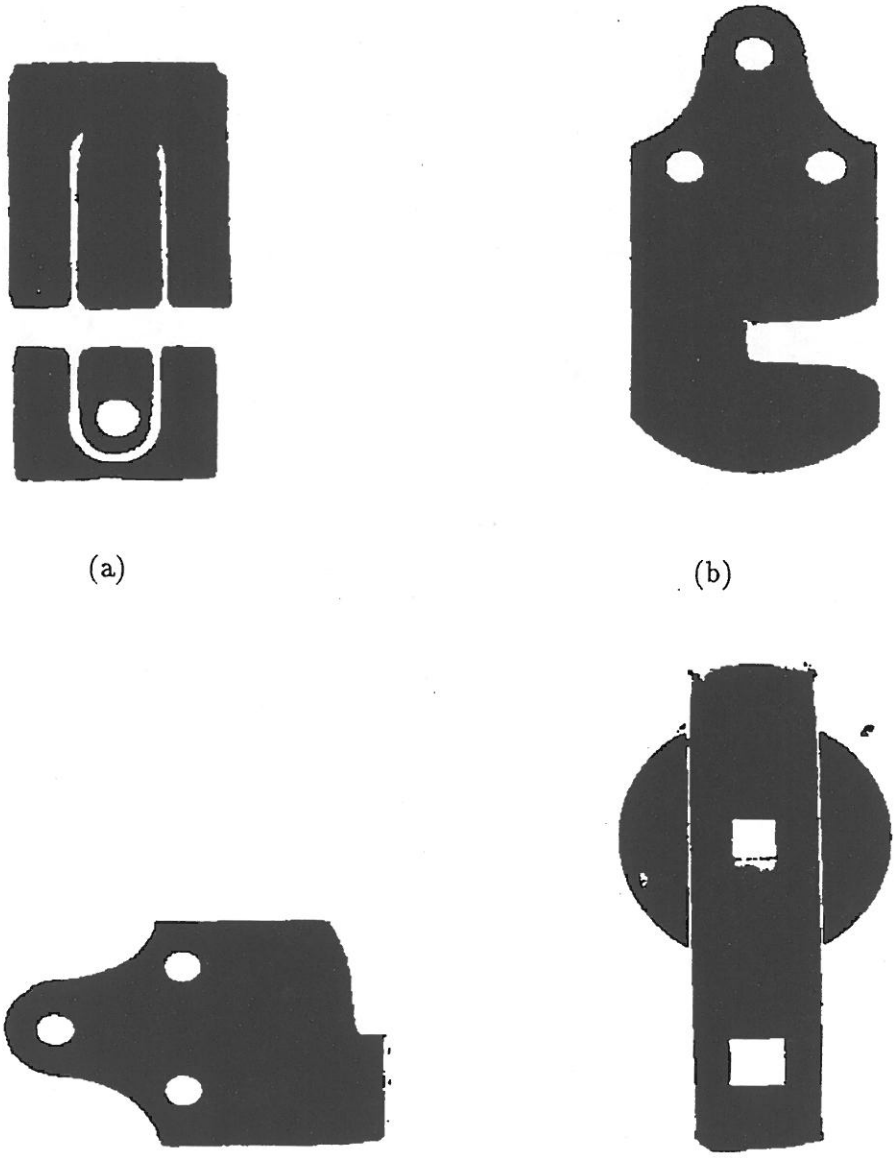

(a) (b)

(c) (d)

Figure 3: Machine part images. (a) Part 1. (b) Part 2. (c) Part 3. (d) Part 4.

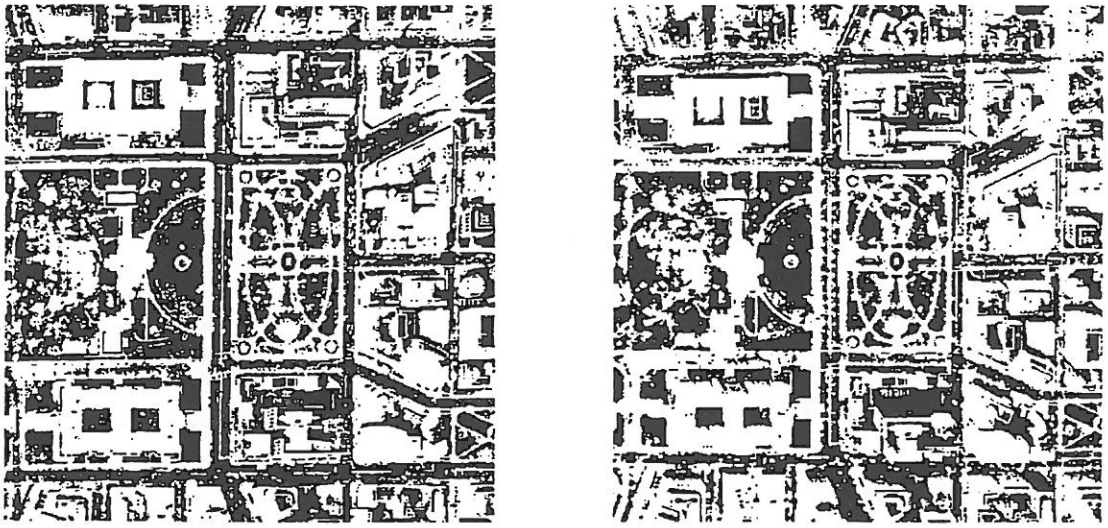

(a) (b)

Figure 4: Aerial images of Washington DC. (a) D.C. 1. (b) D.C. 2.

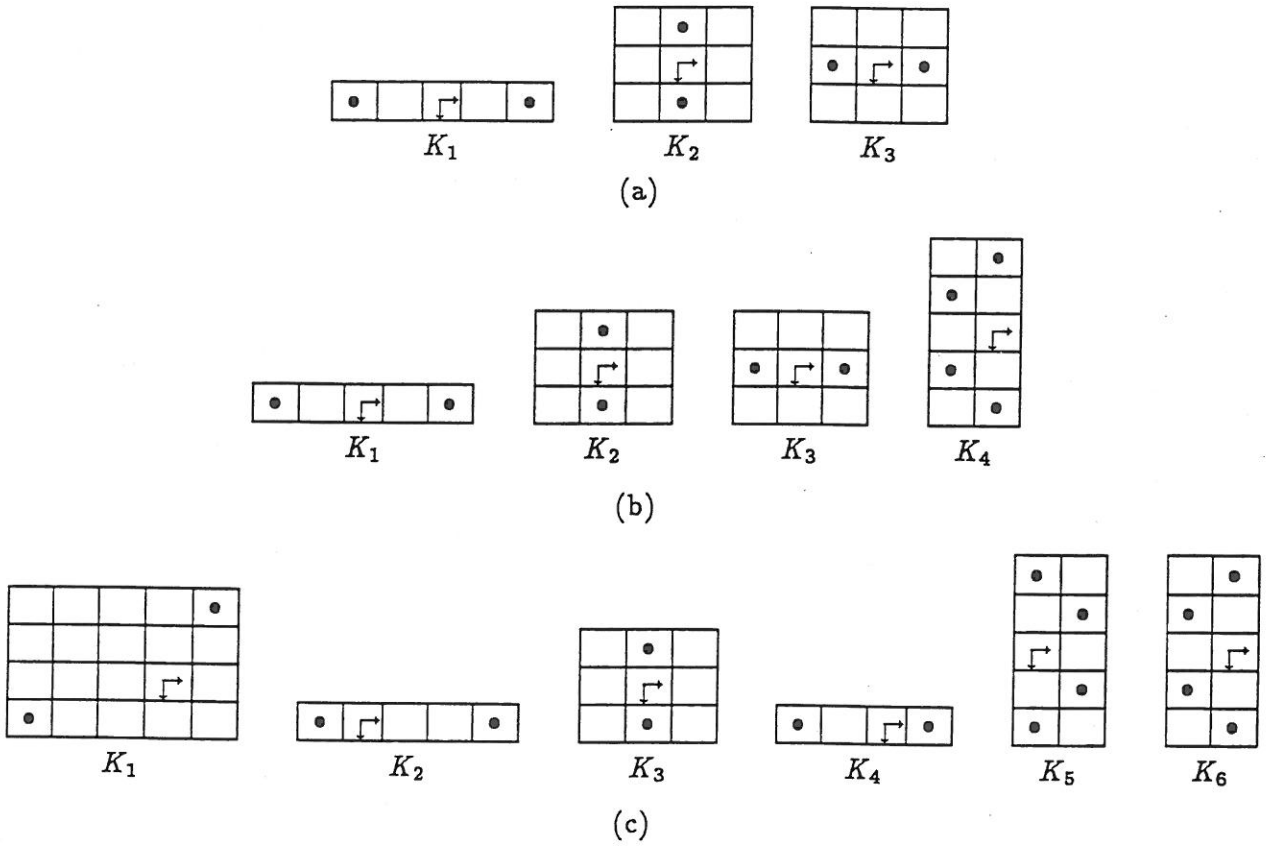

Figure 5: Union of erosions filters for machine part images. (a) $N_D = 0.05$. and $N_D = 0.10$. (b) $N_D = 0.15$. (c) $N_D = 0.20$.

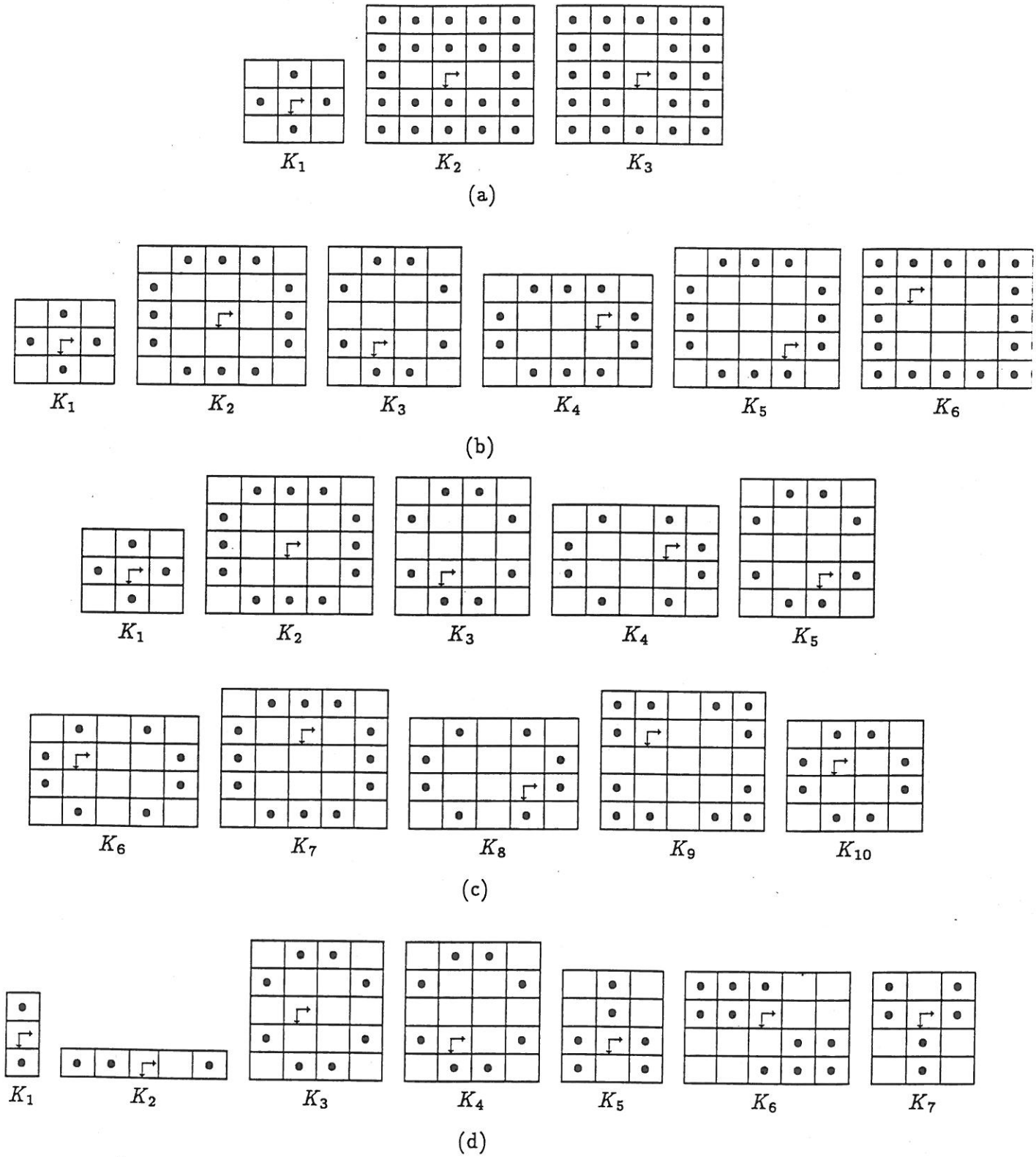

Figure 6: Union of erosions filters for D.C. images. (a) $N_D = 0.05$. (b) $N_D = 0.10$. (c) $N_D = 0.15$. (d) $N_D = 0.20$.

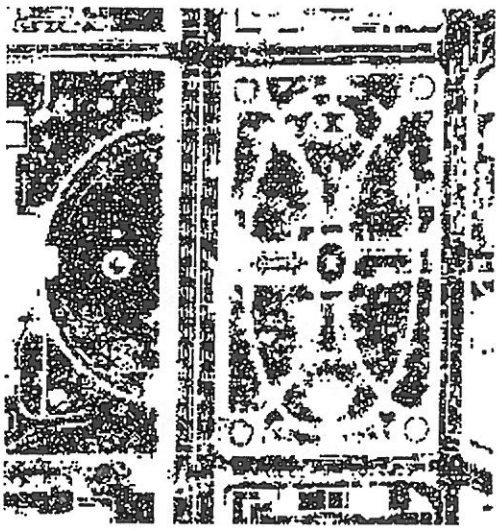

(a)

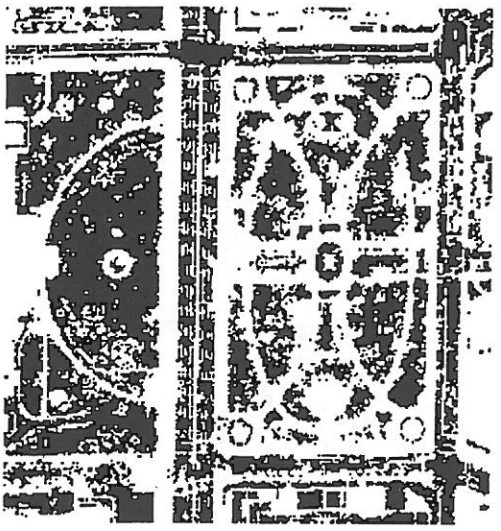

(b)

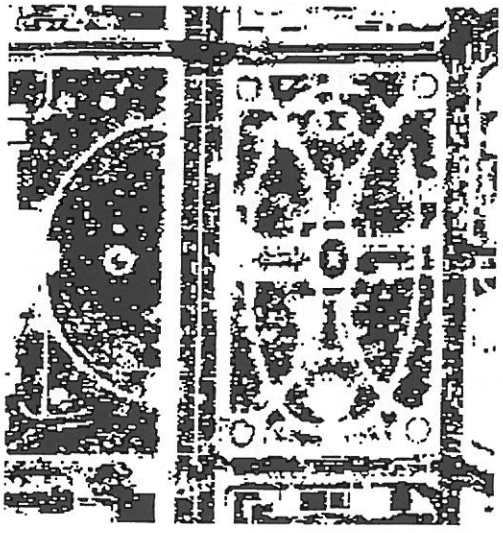

(c)

(d)

Figure 7: Filtering example with 256 × 256 center section of D.C. 1 image and $N_D = 0.15$. (a) Noisy image. (b) Noisy image filter by union-of-erosions. (c) Noisy image closed by a 2×1 line. (d) Blowup of a 63×63 pixel section: upper left original image, upper right noisy image, lower left image filtered by a union-of-erosions, and lower right image closed by a 2×1 line.

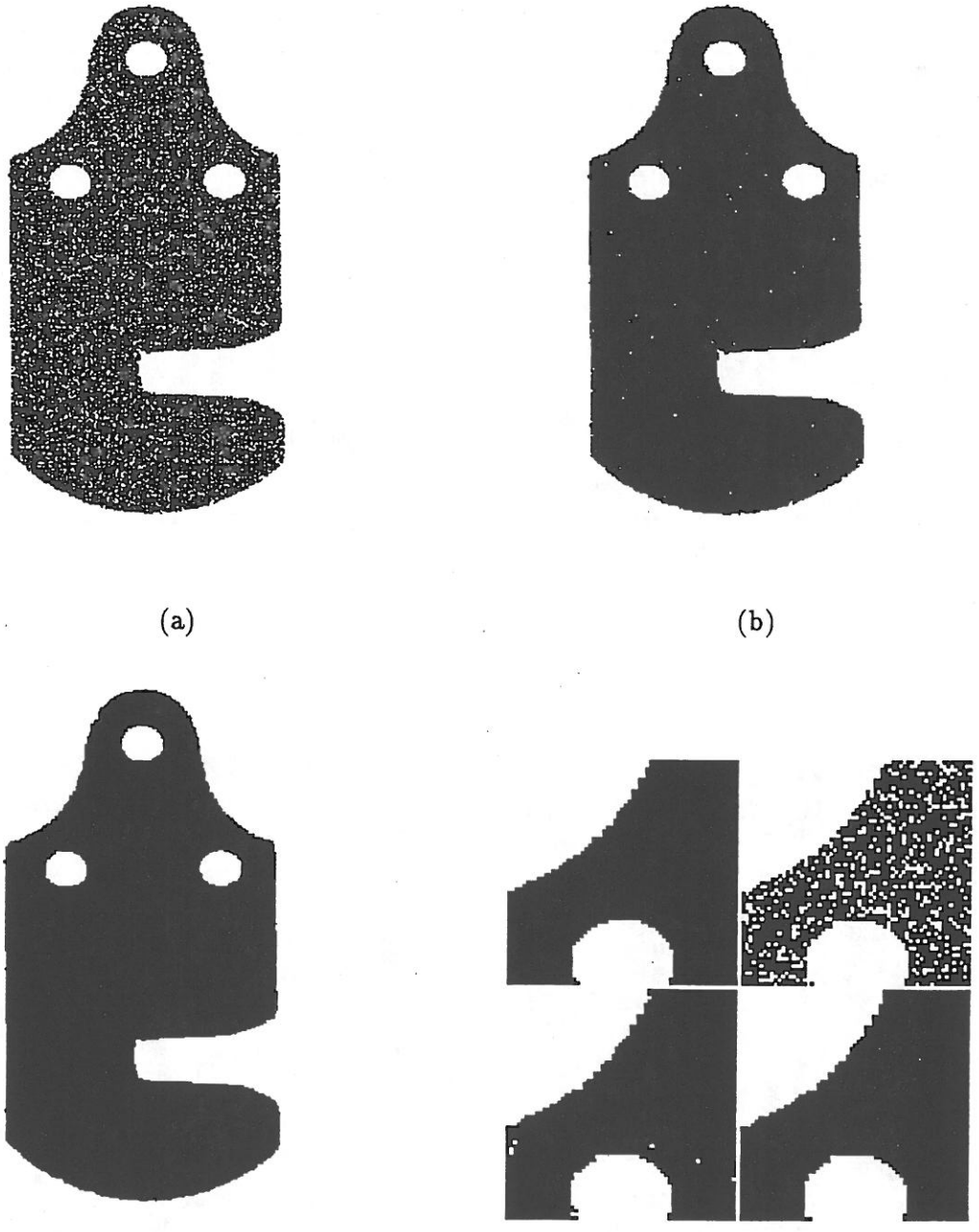

Figure 8: Filtering example with Part 2 and $N_D = 0.20$. (a) Noisy image. (b) Noisy image filtered by union-of-erosions. (c) Noisy image closed by a 4×4 square. (d) Blowup of a 63×63 pixel section: upper left original image, upper right noisy image, lower left image filtered by a union-of-erosions, and lower right image closed by a 4×4 square .

Image	Noise density N_D	Noisy image error $e(F,\tilde{F})$	UOE Filtered image error $e(F,F_F)$	Closed image error $e(F,F_C)$	Normalized filtered image error $\frac{e(F,F_F)}{e(F,\tilde{F})}$	Normalized closed image error $\frac{e(F,F_C)}{e(F,F_N)}$
D.C. 1	0.05	5314	3783	$*$ 6614	0.7120	1.2448
	0.10	10668	7009	$*$ 8790	0.6570	0.8240
	0.15	16065	10467	$*$ 11616	0.6515	0.7230
	0.20	21547	13333	$\star$ 13595	0.6118	0.6309
D.C. 2	0.05	4715	3303	$*$ 5199	0.7005	1.1025
	0.10	9462	6118	$*$ 7170	0.6466	0.7579
	0.15	14260	9138	$*$ 9795	0.6408	0.6869
	0.20	19024	11241	$\star$ 11212	0.5909	0.5894
Part 1	0.05	1974	43	$\star$ 35	0.02172	0.01783
	0.10	3977	91	$\diamond$ 63	0.02296	0.01582
	0.15	5952	166	$\diamond$ 88	0.02781	0.01472
	0.20	7980	227	$\diamond$ 116	0.02841	0.01453
Part 2	0.05	2239	42	$\diamond$ 37	0.01871	0.01643
	0.10	4543	98	$\diamond$ 58	0.02165	0.01279
	0.15	6805	165	$\diamond$ 84	0.02424	0.01231
	0.20	9117	236	$\circ$ 110	0.02594	0.01209
Part 3	0.05	1618	29	$\star$ 25	0.01761	0.01544
	0.10	3260	74	$\diamond$ 51	0.02279	0.01555
	0.15	4875	128	$\diamond$ 69	0.02617	0.01419
	0.20	6516	172	$\diamond$ 84	0.02639	0.01294
Part 4	0.05	2083	162	$\bullet$ 84	0.07766	0.04039
	0.10	4158	202	$\triangleright$ 145	0.04855	0.03494
	0.15	6309	291	$\triangleright$ 223	0.04617	0.03760
	0.20	8393	487	$\triangleright$ 433	0.05808	0.05162

Closing types

$*$ 2×1 line
$\star$ 2×2 square
$\diamond$ 3×3 square
$\circ$ 4×4 square
$\bullet$ 1×3 line
$\triangleright$ 1×4 line

Table 1: Experimental results.

Image	Noise density N_D	Expected net fixes $E[e(F,\tilde{F}) - e(F,F_F)]$	Actual net fixes $e(F,\tilde{F}) - e(F,F_F)$
D.C. 1	0.05	1333	1530
	0.10	3439	3659
	0.15	5882	5599
	0.20	7830	8214
Part 1	0.05	1957	1931
	0.10	3860	3885
	0.15	5888	5787
	0.20	7904	7753

Table 2: Cost function and the net number of fixes.